Author/s:
Segeritz, P;Kolesnik, K;Scott, DJ;Collins, DJ

Title:
Quantitative mechanical stimulation of GPR68 using a novel 96 well flow plugin

Date:
2024-03-21

Citation:
Segeritz, P., Kolesnik, K., Scott, D. J. & Collins, D. J. (2024). Quantitative mechanical stimulation of GPR68 using a novel 96 well flow plugin. Lab on a Chip: miniaturisation for chemistry, physics, biology, materials science and bioengineering, 24 (6), pp.1616-1625. https://doi.org/10.1039/d3lc00767g.

Persistent Link:
https://hdl.handle.net/11343/343937

Quantitative mechanical stimulation of GPR68 using a novel 96 well flow plugin

Philipp Segeritz[1,2], Kirill Kolesnik[1], Daniel J. Scott[2,3*], David J. Collins[1,4*]

[1]Department of Biomedical Engineering, The University of Melbourne, Parkville, VIC 3010, Victoria, Australia

[2]The Florey Institute of Neuroscience and Mental Health, The University of Melbourne, 30 Royal Parade, Parkville, VIC 3052, Australia.

[3]Department of Biochemistry and Pharmacology, The University of Melbourne, Parkville, VIC 3010, Australia

[4]The Graeme Clark Institute, The University of Melbourne, Parkville, VIC, 3010, Australia

*Corresponding Authors: Daniel J. Scott, David J. Collins

Email: daniel.scott@florey.edu.au, david.collins@unimelb.edu.au

Author Contributions: P.S. performed the experiments and fabricated devices. K.K. performed simulations. D.J.S and D.J.C contributed to supervision, conceptualization, and planning. All contributed to writing.

Keywords: Microfluidics, GPR68, mechanobiology, mechanosensitive protein, protein analysis

Abstract

Mechanosensitive proteins play a crucial role in a range of physiological processes, including hearing, tactile sensation and regulating blood flow. While previous work has demonstrated the mechanosensitivity of several proteins, the ability to apply precisely defined mechanical forces to cells in a consistent, replicable manner remains a significant challenge. In this work we present a novel 96-well plate-compatible plugin device for generating highly-controlled flow-based mechanical simulation of cells, which enables quantitative assessment of mechanosensitive protein function. The device is used to mechanically stimulate HEK 293T cells expressing the mechanosensitive protein GPR68, a G protein-coupled receptor. By assaying intracellular calcium levels during flow-based cell stimulation, we determine that GPR68 signalling is a function of the applied shear-force. As this approach is compatible with conventional cell culture plates and allows for simultaneous readout in a conventional fluorescence plate reader, this represents a valuable new tool to investigate mechanotransduction.

Introduction

Mechanosensation plays a crucial role in a range of biological processes, including hearing(1), flow sensing(2) and homeostasis(3). During these biological processes mechanosensitive proteins, expressed on the surface of relevant cells, detect the cellular micromechanical environment to generate adaptive cellular responses. Over the last decade several mechanosensitive proteins have been identified and studied. The mechanosensitive channel of large conductance (MscL), for instance, is a bacterial ion channel that opens in response to membrane tension to protect *Escherchia coli* (*E. coli*) from osmotic shock(4) and can conduct water, ions and even small proteins(4–6). In mammalian cells mechanosensation is enabled by a range of mechanosensitive proteins, including ion channels such as: Piezo1 and Piezo2(7), the two-pore-domain potassium channels TREK-1, TREK-2 and TRAAK (8–11) and the transient receptor potential channels (TRPCs) such as TRP-4 (12–14). Although computational studies and knowledge of protein structure have elucidated potential mechanisms of mechanosensation for these ion-channel proteins (7,15–17), the mechanosensitivity for many of these proteins remains poorly understood on the molecular level. More recently, the mechanosensitive G protein-coupled receptor (GPCR) GPR68 has been identified as a non-ion channel mechanosensitive protein, which upon mechanical activation triggers intracellular G protein-coupling and the activation of diverse intracellular signaling responses that act on a longer timescale to ion channels(18). GPR68 is expressed in a wide range of human cells and tissues(19), including the intestinal tract, gastric glands and in muscle layers of arteries and arterioles, and capillaries(20). In addition to its suspected role in mechanosensation and flow modulation, GPR68 has been shown to be an important pH sensor and modulator(21). In line with GPR68's role as pH sensor, this mechanosensitivity is further pH dependent(22). GPR68 expression is also upregulated in various tumor cells, where it is believed to play crucial roles in tumor biology(19). Acidosis is highly prevalent in the tumor microenvironment and makes GPR68 an interesting potential therapeutic target(19). In terms of mechanosensitivity, GPR68 can sense shear stress when expressed in HEK 293T cells and is required to sense shear stress in rat endothelial cells, and its activation leads to dilation of Small-Diameter Mesenteric Arteries, therefore identifying GPR68 as an essential flow sensor for cardiovascular function(18). While this is a crucial step, more precise quantification of the forces required to activate GPR68 is needed to better understand its mechanosensitivity and the physiological role it plays.

This lack of a quantitative understanding of the relationship between micromechanical forces and cellular responses is not limited to GPR68, where the specific mechanisms underlying most mechanosensitive proteins remain poorly understood. A reason for this lack of quantitative knowledge relates to the challenges associated with applying defined mechanical stimuli to living cells and accurately measuring real-time cellular responses. A diverse range of mechanical stimuli have been previously used to determine mechanoresponses in cells, though each comes with their own challenges. Patch clamp pipettes for instance, can be used to generate pressure differences, inducing bending stress on cell membranes(23,24). This approach can record cellular responses in a very precise manner, but due to the time-consuming process of patching single cells it is limited to low throughput assays. Ultrasound-based approaches using acoustic waves as a mechanical stimulus can perform higher-throughput analysis via stimulation of larger numbers of cells(25–28), though acoustic fields also simultaneously create flow via acoustic streaming. This results in challenges around determining the magnitude and type of stimulation cells are subjected to and decoupling their effects, as ultrasound stimulations are also accompanied by flow-mediated shear forces arising from acoustic streaming. Flow chambers on the other hand provide a simple and straightforward method to apply hydrodynamic forces (29–31), though the generation of homogenous and well-defined shear forces remains difficult, and where it is challenging to combine these methods with conventional cell culture tools. Work from Xu et al., for instance, highlights both the potential and drawbacks of current flow-based stimulation approaches, where an array of 384 undulating pins was utilized, creating disturbed flow in wells of a 384 well plate (18). While this system generates flow around cells, and thus microscale shear stresses within microwells, the multidirectional, nonuniform and dynamic nature of such flow does not allow for a precise estimation of the shear stress generated. Further, the use of ultrasound has potentially confounding effects, where the same oscillations that generate acoustically-driven flow also generate pressure waves which may independently impact mechanosensitivity.

In this work we present a microfluidics-inspired approach that enables the generation of defined microscale forces on living cells in a microtitre plate. The plugin device we demonstrate allows the determination of the specific cellular responses to shear stresses independent of other stimulation mechanisms, which we utilize to measure the sensitivity of the vascular flow sensor, GPR68, to shear stress in living cells. The approach we present here thus represents a valuable new mechanotransduction investigation tool, with the ability to make quantitative assessments of cells expressing flow-sensing proteins such as GPR68 using standard biological laboratory apparatus.

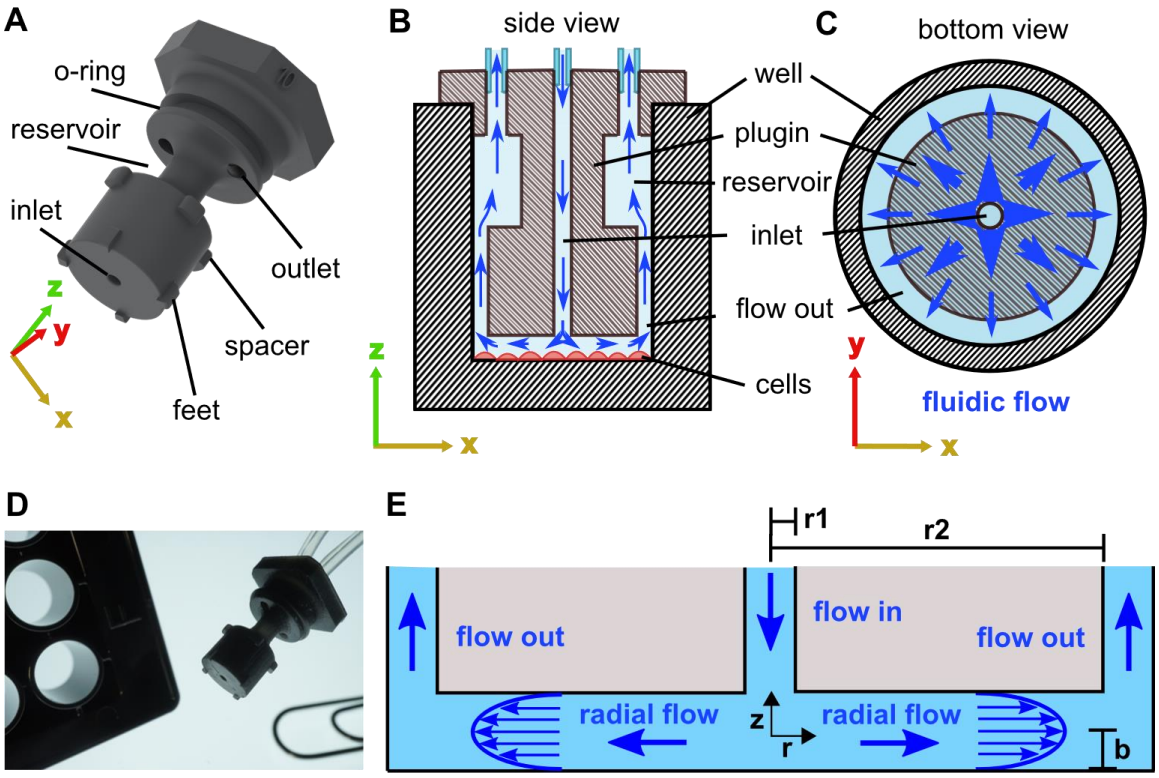

Figure 1: System design. **(A)** Rendering of flow plugin illustrating inlets, outlets, and spacers. **(B)** Schematic of flow in a well with plugin inserted, side view. **(C)** Bottom view. **(D)** Photograph of plugin, 96 well plate and paper clip for scale. **(E)** Schematic of flow at the bottom of a well with the plugin flow device inserted, illustrating relevant parameters to calculate flow velocity and shear rate, including inlet radius r_1, plugin radius r_2 and channel height 2b.

Principles and System Design

A novel flow plugin for mechanical stimulation in 96-well cell culture plates

A flow plugin device is designed (Figure 1A) to administer controlled flow within a single well of a microtitre plate, within which mammalian cells are adhered to the bottom surface of the well. In this design fluid is administered through an inlet to the centre of the cell-harboring surface of the well, from which the injected fluid flows radially outward over the cells before being evacuated from the well through outlets running parallel to the wall of the well, as illustrated in Figure 1B. The terms inlet and outlet are used here in reference to the volume containing the cells, enclosed by the plugin and the well.

The return path is further designed such that the fluidic resistance, and thus flow velocity, is the same regardless of where on the periphery of the well the fluid exits. Here 200 µm tall spacers at the bottom of the design ensure a constant distance from the bottom of the well to the plugin and

create a small, sub-millimeter high "cell chamber". The device depicted in Figure 1 is designed to fit a 96 well cell culture plate, for which each well has a well diameter of 6.58 mm at the bottom of the well. The bottom of the device has a diameter of 5.7 mm, resulting in a 440 μm wide peripherical run-off gap for fluid egress. This run-off gap acts as a fluidic resistance domain, which when combined with a reservoir immediately succeeding it, homogenizes the fluid velocities across different well angles and ensures uniform run off along the borders of the well and out of the device through two discrete outlets, placed off-center on either side at the top of the reservoir. The device is designed to create a radial flow field within the cell chamber domain, with the flow velocities and thus shear rates being inversely proportional to radial position on the surface (Figure 1C), enabling the response of a cell population to a range of known flow velocities to be simultaneously assessed. The design is fabricated with a DLP (Digital Light Processing) 3D printer, facilitating the generation of unique and complex 3D geometries, readily enabling the iterative prototyping and integration of these devices with conventional well plate geometries. Figure 1D shows a photograph of the printed device, including a 96-well plate and a paperclip for scale. The device dimensions can be adapted for different cell culture plates or desired channel heights and, while we characterize and demonstrate the utility of this device within a single well of a 96 well plate, the design concept is highly amenable to scaled, multiplexed analysis in multi-well platforms.

Flow velocities and shear rates

To determine the magnitude of the mechanical stimulus cells would experience in the device depicted in Figure 1A-C, flow velocities and shear rates within this system can be analytically determined(32). Figure 1E illustrates the flow at the bottom of a well containing the designed plugin, with relevant dimensions including the inlet radius r_1, the plugin radius r_2 and the channel height $2b$. The shear stress within such a system can be determined by

$$\tau = -2z\,\mu\,\frac{3Q}{8\pi b^3 r}, \tag{1}$$

where τ is the shear stress, r is the radial distance of center at any given point, z is the position in the z-direction, b is the half channel height, μ is the viscosity of the fluid medium, and Q is the volumetric flow rate. This enables the calculation of shear stress at arbitrary planes within the well for a given injected volumetric flow rate. We utilize Equation 1 to benchmark simulation results, both of which are presented in Figure 2.

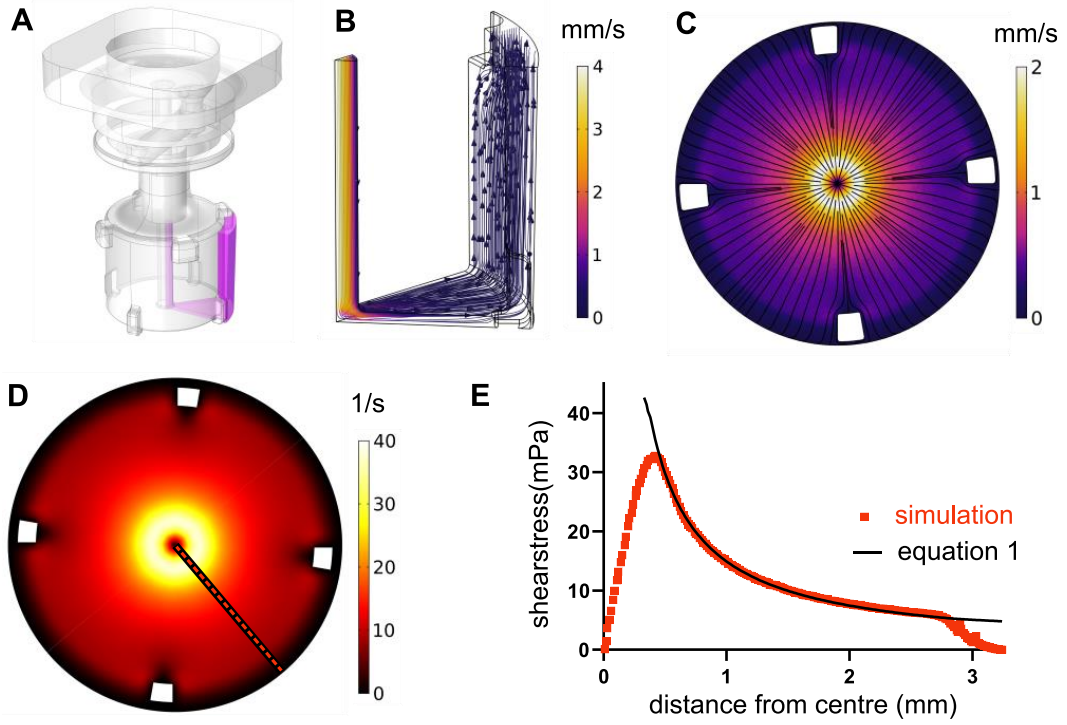

Figure 2: Flow velocity and shear rate simulations for the plugin device inserted in a 96-well plate well. Injection rate 50 µl/min and inlet diameter 750 µm, plugin diameter 5.7 mm, well diameter at bottom 6.58 mm, and viscosity 0.75 Pas. **A**) Fluidic simulation domain and its spatial relation to the plugin. **B**) Flow velocity field in the fluidic domain. **C**) Bottom view of flow velocities in central plain (measured at z = 100 µm). **D**) Bottom view of shear rates at the bottom of the well (measured at z = 0 µm). **E**) Plots of simulated shear stress along the dotted line in (D) with analytically calculated shear stress.

Results and Discussion

Simulating flow velocities and shear rates

Computational fluid dynamics (CFD) analysis is performed on the design from Figure 1A-C to model the fluid flow and shear stress at the bottom of the well, both to validate Equation 1 and to determine the impact of the finite-width inlet and supporting spacers on the flow profile. CFD analysis is further useful to determine the effect of the finite-width central flow outlet/inlet. Flow velocities and corresponding shear rates are simulated using COMSOL Multiphysics 5.5 (COMSOL, Stockholm, Sweden) (See Supplementary Note S1). CAD files of the fluidic domain were created based on the device depicted in Figure 1A-C and the topology of a well in a 96-well plate. The simulation excluded the presence of cells, as their small dimensions and flattening in an

adherent state (<5 µm high), suggests minimal impact on the overall flow trajectories. Due to the radial symmetry of the device and the presence of four radially equidistant spacing elements, only one-eighth of the domain is directly simulated, with a symmetry boundary condition used to represent the entire domain. Figure 2A shows this modelled fluidic domain in its relation to the plugin device. Here we simulate the injection of aqueous fluid (viscosity = 0.75 Pas) at a rate of 50 µl/min. The resulting simulated flow velocities are depicted in Figure 2B, ranging from 4 mm/s in the middle of the central inlet to an order of magnitude lower in the peripheral outflow areas. The highest flow velocities for a given radial position are observed 100 µm above the bottom surface (halfway up the 200 µm chamber height) and are depicted in Figure 2C. Within the flow chamber itself, the highest such velocities occur towards the central well area (up to 2 mm/s), with a local stagnation zone immediately below the central outlet/inlet. A reduction of the fluid velocity is further observed towards the edge of the well. As expected, the bottom spacers locally disturb the radial fluid flow as fluid moves around them, though their influence on flow velocities and direction is limited to their direct vicinity.

To further assess the shear forces cells may experience, the fluid shear rate at the bottom surface of the well is shown in Figure 2D. As the inlet in the centre of the well has a finite diameter, the radius at which maximum surface flow velocity occurs is displaced from the well centre. Well shear rates peak at 43.5 s^{-1}, at ~375 µm from the centre of the well, corresponding to the outer radius of the inlet channel. Here the injected fluid flows from the central inlet into the disk-shaped channel region between the bottom of the well and the flow plugin. The well bottom shear rate then decreases with increasing radius from the central inlet. A further reduction in shear rate occurs close to the edge of the well, at the upper boundary extent where the fluid flow transitions from radial to vertical, with fluid exiting the radial flow area and being directed towards the reservoir. Within the disk-shaped channel region, the simulated shear rate accords with that predicted by Equation 1, where the dashed line in Figure 2D denotes the axis along which this quantity was measured in Figure 2E. Here the shear stress can be calculated from the shear rate using $\tau(r) = \dot{\gamma}(r) * \mu$, where τ is the shear stress and $\dot{\gamma}$ is the shear rate, both being a function of the radial position. The highest shear stresses are thus observed directly next to the inlet, with a maximum of 0.04 N/m^2 (40 mPa) for the flow rate and dimensions used in this simulation, where shear stress and shear rate scale linearly with increasing flow rate and inversely with increasing height of the disk-shaped channel region. With increasing distance from the inlet, the shear stress drops until

reaching ~5 mPA at a radial distance of 2.85 mm, evidencing an order of magnitude variation in applied shear stress across the well bottom. Deviations from the analytical results here, specifically in the vicinity of the inlet and outlet regions, are a result of the incorporation of a fixed-width inlet and vertical return flow at the edge of the system in the physical device.

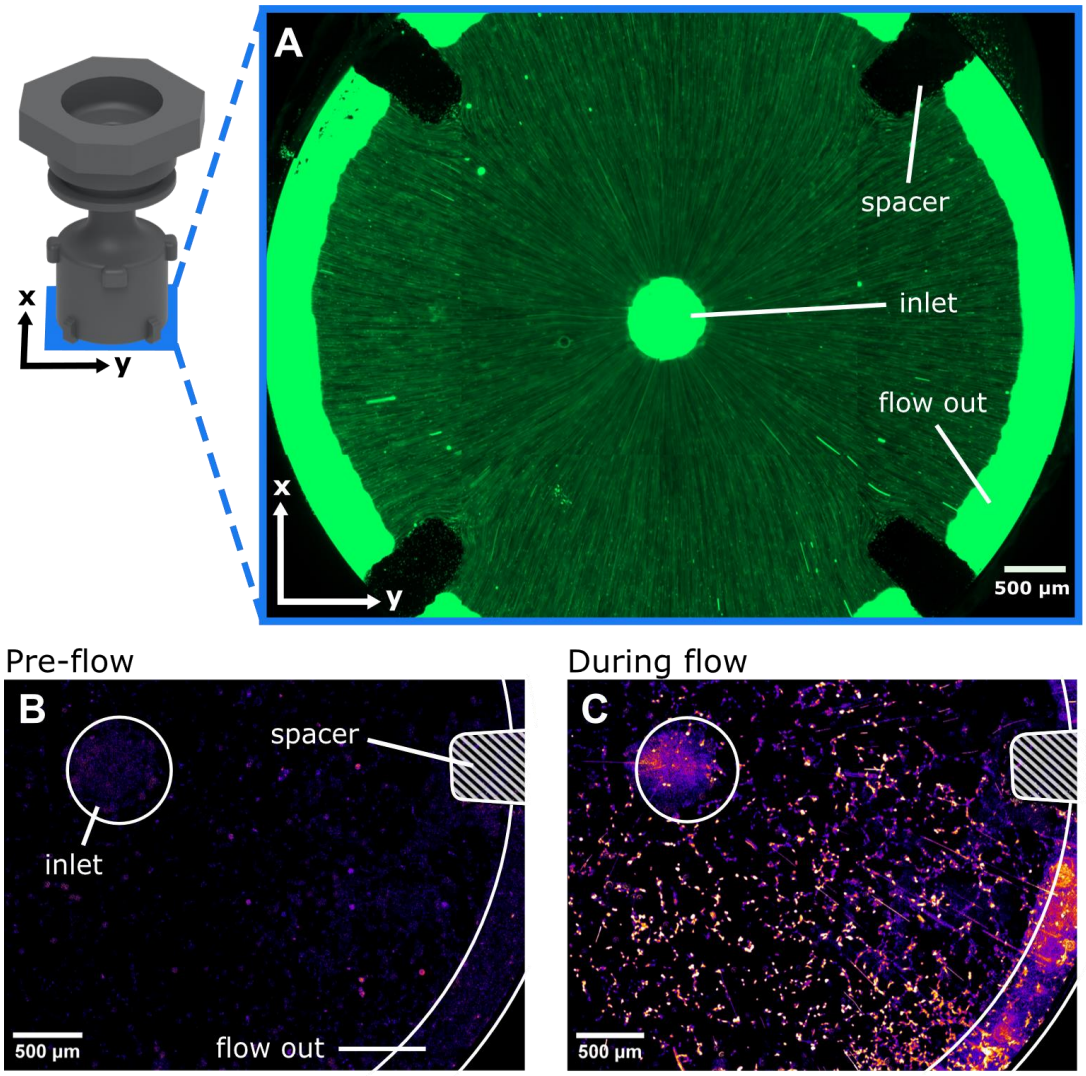

Figure 3: Flow visualization of fluorescent particles in flow. Images are viewed from the bottom, with spacer height 200 µm and injected flow 50 µl/min. **A**) Flow visualized with 1µm green, fluorescent spheres (stitched image of 16 tiles). **B,C**) Calcium induced fluorescence in HEK R-GECO1 GPR68 cells before (t=20s) and during (t=40s) flow. Demonstrating the presence of flow, 5 µm red fluorescent spheres traces are visible in **(C)**.

Flow verification and visualization with fluorescence particles

To experimentally verify the fluid flow created with our designed plugin the 3D printed device is inserted into the well of a 96 well plate and a 0.0025 % solution of 1 µm green fluorescent microparticles injected into the plugin at a 50 µl/min flow rate. Images of the flow chamber immediately above the bottom surface of the well are recorded using an inverted fluorescence microscope. Long exposure (1000 ms) images show microparticle flow as lines radiating from the central inlet, albeit with flow deviations as the particle solution flows around the spacer elements near the periphery of the plugin, and is consistent with the expected CFD-derived flow trajectories from Figure 2. Here Figure 3A presents 16 merged images (4x4 tiles) that depict the entire bottom flow chamber created by the plugin, as viewed from the bottom. The central inlet, the peripheral outlet and the bottom spacers are visible here as bright green or black respectively, this being a function of the number of particles present above a given location. While this method precludes a straightforward assessment of the generated flow velocities due to the unknown z-position of individual particles as viewed from the bottom of the well, it offers an overview of the flow field within the device, with the apparent particle trajectories radiating from the plugin centre in line with the simulation results from Figure 2C.

In sum, the calculations, stimulations, and observations demonstrate that the plugin device generates a well-defined laminar flow whose characteristics (shear rate, flow velocity, shear stress) are a function of the radial position. Shear rates at different points on the bottom of the well, where this is a linear function of the applied flow rate, can readily be adjusted. This shear rate variation further enables the simultaneous investigation of different shear stresses in the same well using a single flow rate, whether using optical microscopy to measure the entirety of the well area or using orbital scans in a plate reader system.

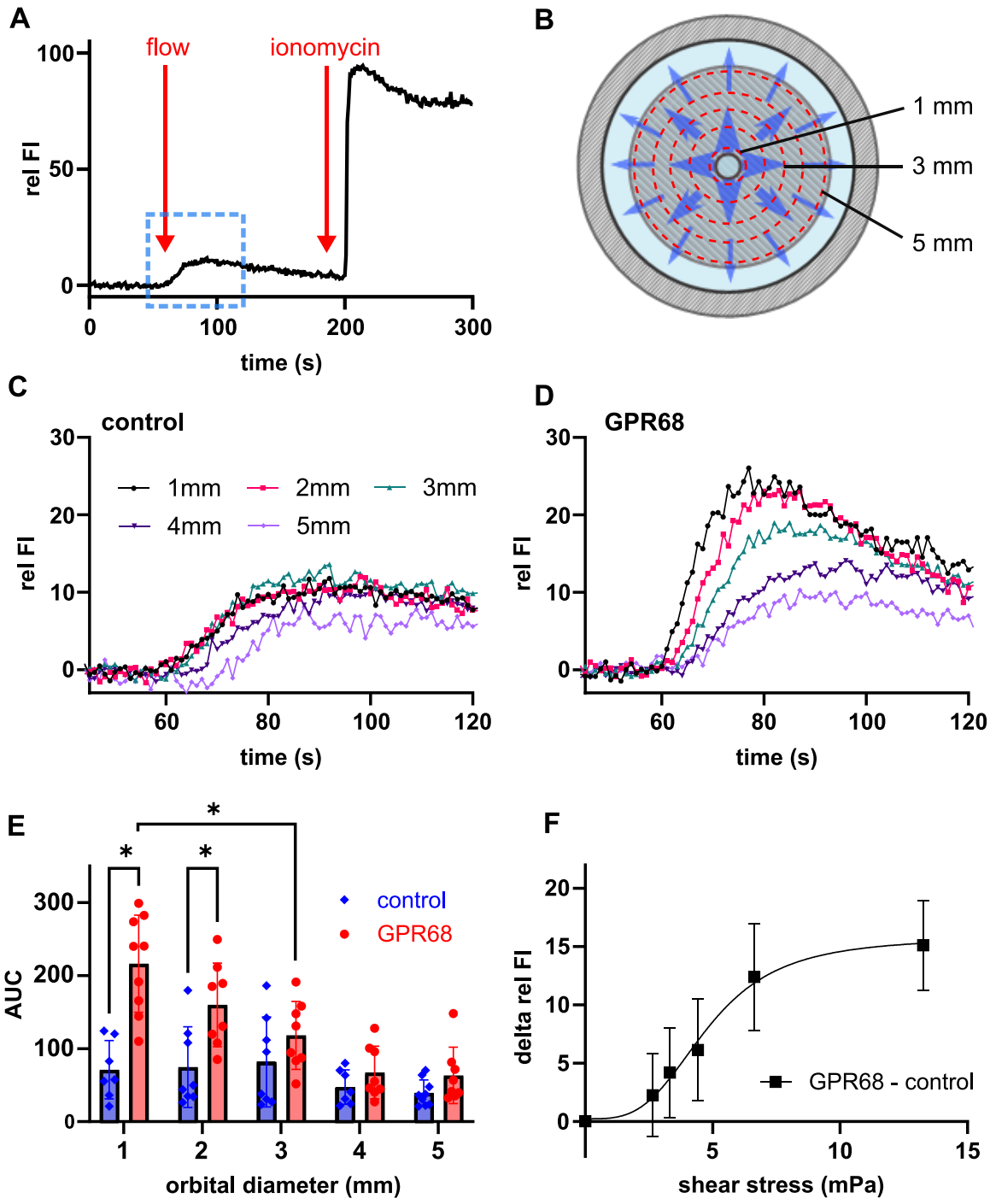

Figure 4: Quantifying the response of GPR68 to shear rate. (**A)** Example recording of relative fluorescence in fluorescence plate reader demonstrating flow and ionomycin response. Flow stimulation is applied after 50 seconds of baseline recording and 5 uM ionomycin is applied after 200 seconds. The baseline is averaged and subtracted, before the data is normalized to the maximal ionomycin response. (**B)** Diameters around the central inlet along which orbital measurements are

recorded (bottom view). (**C,D)** Flow responses of HEK-293 cells stably expressing the calcium indicator R-GECO1 (control) and the mechanosensitive protein GPR68 co-expressed with R-GECO1 (GPR68) measured at different orbital diameters. Here a channel height of 600 µm is used in combination with an injection rate of 200 µl/min. A total of 8 independent recordings are performed for each diameter and each cell group, recording a single well at a time to increase the temporal resolution. To quantify the flow response the area under the curve (AUC) for $50 < t < 100$ is calculated. Averages are displayed in **(E**), with error bars indicating the standard error. Two-way ANOVA identifies both diameter ($p = 0.0002$) and GPR68 expression ($p < 0.0001$) as highly significant sources of variation. (**F**) Maximal flow responses for $50 < t < 100$ are calculated and the average control group maxima subtracted from the GPR68 group to determine the GPR68-dependent response. Results are plotted against the shear stress corresponding to different diameters as determined by Eqn. 1. and fitted with a nonlinear regression curve.

Flow mediated activation of the mechanosensitive protein GPR68

To demonstrate the utility of our novel flow plugin we quantify the shear-dependent response of the mechanosensitive protein GPR68, a relatively poorly characterised mechanosensory protein, in living human-derived cells. GPR68 is a GPCR that can sense flow and plays an essential role in vascular physiology(18). Although mechanosensitivity of GPR68 has been demonstrated(18,33), the force vs. response curve of this protein has not been accurately quantified. Previous work, for example, used flow-stimulating apparatus that did not generate defined local flow velocities on the GPR68-expressing cells, making it difficult to assign accurate force vs. response characteristics.

GPR68, as with many other G protein-coupled receptors, mobilizes intracellular calcium upon activation(18,34). We therefore used intracellular calcium concentration as a proxy for receptor activation. To enable real-time measurement of intracellular calcium signalling, a HEK 293T cell line stably expressing GPR68 and the genetically encoded calcium sensor R-GECO1 was created via lentiviral transduction (see Methods). A HEK 293T cell line stably expressing only R-GECO1 is used as a GPR68-null control. Both GPR68 and control cells were seeded into clear bottom, black-walled 96 well culture plates and 24 hours after seeding a 3D printed flow plugin was inserted into wells to enable flow stimulation. To directly visualize the impact of flow on cellular responses, the culture plate and flow plugin apparatus was placed in a live-cell imaging microscope. R-GECO1 fluorescence was recorded before, during and after a 20 second flow stimulus of 50 µl/min. Clear increases in cellular R-GECO1 fluorescence was observed upon flow stimulation. Figure 3B depicts the R-GECO1 fluorescence of GPR68-expressing cells in the flow apparatus before initiation of flow, whereas Figure 3C presents the R-GECO1 fluorescence of the same GPR68-expressing cells after 20 s of flow. Supplementary Video 1, included as an attachment, further illustrates this transient flow response.

While microscopy is useful to confirm cellular responses and demonstrate that these effects are due to flow, to quantify the flow-dependent responses and do so in an automated, reproducible way, a fluorescent plate reader was used to measure responses of cells in a microplate. R-GECO1 fluorescence in the cells is monitored at a rate of 1 Hz before, during and after a 20-second-long flow stimulus through the plugins. After flow stimuli, cells are exposed to a solution of 5 μM Ionomycin, administered via a pipette. Ionomycin is a calcium ionophore that triggers G protein-independent release of Ca^{2+} from intracellular stores and thus will trigger a maximal R-GECO1 fluorescence signal in viable cells remaining in the well. The Ionomycin response of cells after flow stimulation serves as a cell viability signal and a way to normalise observed flow-based calcium responses among different cell treatment groups. An example response following this experimental design is presented in Figure 4A. After subtracting the baseline fluorescence from each measured well, the fluorescence intensities at any given time were normalized to the respective maximal Ionomycin response recorded to account for well-well differences in cell density.

Due to the varying cross-sectional areas for different radii in the flow chamber, multiple local flow velocities (and thus shear rates) are generated in the radial flow across the surface of the well where the cells are adhered (Figure 2C-E). We take advantage of this characteristic to measure how cells respond to varying shear force in the same system by measuring cellular R-GECO1 fluorescence at discrete orbital diameters (Figure 4B). To accomplish this, we utilized the orbital averaging capability of a fluorescence plate reader. In this setup, the plate reader captures fluorescence measurements along a circle with a user-defined diameter around the centre of the well. The average cellular Ca^{2+} signalling responses to the flow stimulus at several orbital diameters for the control cells (Figure 4C) and the GPR68 expressing cells (Figure 4D) are presented. Flow-induced calcium signalling is observed in both the GPR68 and the GPR68-null cells, with stronger signals observed for GPR68 expressing cells and an apparent correlation between smaller orbital diameter, and consequently higher shear force and response strength. To further analyse this force vs response relationship the areas under the curves (AUC) are calculated for the time interval from $t = 50s$ to $t = 100s$, which represents the flow injection period (with injections starting at $t = 50s$).

A two-way ANOVA test identifies both diameter ($p = 0.0002$) and GPR68 expression ($p < 0.0001$) overall as statistically highly significant sources of variation. In the GPR68-null control cells, there is no statistically significant difference between the areas under the curves measured at different orbital diameters. In GPR68 expressing cells, cells located at 1 mm orbital diameters display

significantly stronger responses then cells located at orbital diameters of 3 mm ($p = 0.0007$), 4 mm ($p < 0.0001$) and 5 mm ($p < 0.0001$), additionally GPR68 expressing cells located at an orbital diameter of 2 mm exhibit significantly stronger responses than cells located at an orbital diameter of 4 mm ($p = 0.0022$) and 5 mm ($p = 0.001$). When comparing GPR68-null control cells and GPR68 expressing cells located at the same orbital diameter we observe significantly stronger flow responses in GPR68 expressing cells at orbital diameters of 1 mm ($p < 0.0001$) and 2 mm ($p = 0.0002$). As expected, the strongest cellular calcium signals are seen in GPR68-expressing cells located in orbitals closest to the inlet, where flow velocities are the highest.

To better asses the relationship between cell activation and shear stress, local fluorescence maxima in the time interval from t = 50s to t = 100s, corresponding to the application of flow, are plotted against the shear stress values for each orbital diameter (Figure S2). While GPR68-expressing cells clearly exhibit enhanced activation, the control cell population nevertheless showed (lower) flow-based activation. This effect may be explained by activation of endogenous mechanosensitive proteins; here we utilize HEK 293T cells, in which the native expression of mechanosensitive ion channels such as Piezo-1 is well established(35,36) and could account for shear-dependent responses in the control group. To better determine the GPR68-specific flow response, the average maximal flow response displayed by the control group is subtracted from the average maximal flow response displayed by the GPR68-expressing group (Figure 4F). Via non-linear regression fitting we estimate a half maximal GPR68 flow response (ES_{50}) at 4.8 mPa, representative of the protein's shear stress activation level, with increasing activation for higher applied shear rates. While GPR68 stimulation has previously been reportedly at shear stresses as high as between 100 mPa and 2 Pa(18,37), these higher values may be a result of excessive receptor stimulation and/or less precise methods of shear stress estimation that cells experience in their local microenvironment.

Conclusion

We introduce a novel device for quantitative flow-based stimulation in fluorescence plate reader. The device consists of a 3D printable plugin compatible with conventional 96 well cell culture plates, where their combination with a plugin device creates radially expanding laminar flow at the bottom of the well. The radially expanding nature of this flow is predicted by analytical theory and confirmed by simulation and experimental results. This approach thus results in a high degree of control, permitting the shear force to be defined across the bottom of the well, and the simultaneous investigation of different shear forces with a single device and in a cell-culture compatible system.

In contrast to traditional flow cells and chambers, the inclusion of lab-standard standard 96-well plates offers substantial simplifications in tasks such as cell cultivation, media exchange, drug application, and other treatments.

The utility of this device is demonstrated here in the quantitative flow-sensitivity-based investigation of the G protein-coupled receptor GPR68. While the mechanosensitivity of GPR68 has been previously demonstrated(18), here we both isolate the effects of flow from acoustic actuation and quantify the response of GPR68 as a function of shear rate. The ionomycin stimulus serves as a control for variations in cell density and viability and further enhances the precision of the resulting output. We find that transfected HEK 293T cells stably expressing GPR68 consistently exhibit significant stronger responses to flow stimuli than their control counterparts, where the ability to measure cell response as a function of well position permits the analysis of the relationship between applied shear stress and resulting GPR68 activation. This enables the plotting of both cellular responses as a function of known shear stress, as well as determine the threshold shear stress activation for GPR68 (~4.8 mPa). In sum, whereas previous implementations examining mechanosensitive flow responses are limited by the inability to accurately determine local flow-induced forces, preventing a quantitative relationship between applied force and cell response to be determined, the approach presented here represents a pathway towards elucidating these relationships. Moreover, this plugin represents a method that is compatible with existing processes and equipment, utilizing equipment that is readily available in laboratory settings, i.e. plate readers and well plates, making this broadly applicable to cell assays in which control over flow conditions is required.

Materials and Methods

Fabrication

This device was designed in Solid Edge 2021 (Siemens, Germany). Designs were sliced with the slicing software ChiTuBox (ChiTuBox, China) and 3D printed in the Digital Light Processing (DLP) 3D printer Photon Ultra (Anycubic, China). To achieve the highest level of printing precision, feature sizes were designed to be multiples of the layer height where possible. Black Anycubic 3D printing resin (Anycubic, China) was used in combination with a layer height of 20 μm and a 2.5 second exposure time per layer. Finished prints were washed in isopropyl alcohol and cured at a wavelength of 405 nm in a curing station (Anycubic, China). To mitigate the cytotoxic effects associated with the printing resin, the printed devices were subsequently immersed in water

for a duration of 24 hours to minimize the presence of diffusible resin components during flow experiments. While viability and proliferation impacts have been noted in cell cultures over long incubation times(38), effects from the short, second-scale timescales associated with fluid transit through these plugins are not noted here. The plugin bottoms were coloured with black dye to reduce autofluorescence and a coating of poly-D-lysin was applied to reduce hydrophobicity and prevent bubble formation. To ensure uniform dimensions, optical assessments of the channel height formed between the plug-in and the well were performed at three designated positions along the outer boundary of the plug-in. The deviation of height across these points is observed to be less than 5%.

Microscopy and particles

Microscopy images were taken on the Inverted Fluorescence Microscope Axio Observer Z1 (Zeiss, Germany) with Zen pro software and Inverted Fluorescence Microscope IX73 (Olympus, Japan) with CellSens software using GFP filter-sets (green particles) and m-Cherry filter sets (red particles and cells). Green fluorescent microspheres (1.1 μm) and Red fluorescent microspheres (5 μm) Magsphere (Magsphere, California, USA) were used to visualize fluid trajectories.

Cell culture

A HEK 293T cell line stably expressing the calcium sensor R-GECO1 is utilized for this work. The cell line is generated via adenoviral transductions followed by purification via fluorescence activated cell sorting. Using a pCSC vector backbone, a construct containing GPR68 and IRES-XFP vas created. This construct is integrated into the HEK 293T R-GECO1 cell line using adenoviral transduction. The cells are sorted for both R-GECO1 fluorescence and XFP fluorescence using fluorescence activated cell sorting (FACSAria III, BD Biosciences, USA) to obtain a cell line stably expressing both R-GECO1 and GPR68. Cells are grown at 37 degrees Celsius at 5% CO2 in Dulbecco's Modified Eagle Medium supplemented with 10% Fetal Bovine Serum, 100 U/ml Penicillin-Streptomycin and 2 mM L-glutamine (all from Thermo Fischer, USA) and regularly passaged. Prior to stimulation in 96 well plates, cells are seeded into poly-D-Lysin (Sigma Aldrich, USA) coated wells, at a density of around 15,000 cells per well 24 hours prior to the experiments. Cell line source(s): HEKT (internal stock), HEKF- Commercial source, ordered in August 2016 from Invitrogen (Cat #: R790-07). Cells expanded, passaged and many aliquots cryopreserved in 2016. Batch used here was expanded from one of these aliquots, Authentication: N.A. Mycoplasma contamination: Tested upon receiving in 2016, negative. Batch used in this manuscript was not

specifically tested, but cell viability was assayed twice per week upon passaging and culture was always > 85% viable cells.

Microplate photometry

Cells are grown and stimulated in black clear bottom 96 well plates with a standard "chimney well" design (Grainer, Germany, I-No 655090). Measurements are performed in a plate reader model Clariostar (BMG, Germany) at 37°C, a focal height of 4.0, a Gain of 2200 and using an 570 nm filter with 20 nm bandwidth for excitation and an 630 nm filter with a 40 nm bandwidth for emission.

Flow stimulation

A Harvard Apparatus 11 Elite syringe pump (Harvard Apparatus, USA) in combination with 3 ml disposable syringes (Terumo, Japan) is used to generate flow. Plugins and syringes are connected via PTFE thin wall tubing (Cole-Parmer, USA) and silicon tubing connectors. To reduce background fluorescence and for better control over extracellular calcium levels, the DMEM growth medium is exchanged with a custom-made extracellular solution 2 hours before experiments are performed. This solution contains 140 mM NaCl, 2.8 mM KCl, 10 mM hepes, 1 mM MgCl2, 2 mM CaCl2, 10 mM D-glucose and was brought to a pH of 7.4 at room temperature with HCl and NaOH. This extracellular solution is also used for flow stimulation. For the Ionomycin-positive control the plugins are removed, and the cells dosed with 5 μM (final concentration) Ionomycin (Cayman Chemical, USA) in extracellular solution.

Data analysis

The open-source image processing software ImageJ is used to enhance signal visibility in Figure 3B and 3C. Using the image calculator tool, a baseline image (t = 1s) is subtracted from both pre-flow stimulus (t = 20 s) and mid-flow stimulus (t = 40 s) images. The lookup table colormap "Fire" was applied.

Plate reader data is analysed with the help of the graphing and statistics software GraphPad Prism (GraphPad Software, USA). The first 30 seconds of each recoding are used as a baseline. These values are averaged and subtracted from all subsequent values. Subsequently each data set is normalized setting 0 as 0%, and the highest value in each recording as 100%. Including 5 different diameters and 2 sets of cell populations this results in a total of 10 data sets. Each of those 10 contains 8 separate measurements, each of which are normalized to their own baseline and positive

control. The integrated analysis function is used to plot averages, fit curves and to calculate standard errors and areas under the curve for relevant sections.

Acknowledgments

Dr. Collins is the recipient of a Discovery Early Career Researcher Award and Discovery Project from the Australian Research Council (DECRA, DE200100909; DP, DP230102550), and funding from the National Health and Medical Research Council (Ideas, APP2003446).

References

1. Fettiplace R, Kim KX. The physiology of mechanoelectrical transduction channels in hearing. Vol. 94, Physiological Reviews. American Physiological Society; 2014. p. 951–86.

2. Hahn C, Schwartz MA. Mechanotransduction in vascular physiology and atherogenesis. Nature reviews Molecular cell biology. 2009 Jan;10(1):53–62.

3. Zeng WZ, Marshall KL, Min S, Daou I, Chapleau MW, Abboud FM, et al. PIEZOs mediate neuronal sensing of blood pressure and the baroreceptor reflex. Science. 2018 Oct 26;362(6413):464–7.

4. Sukharev S, Anishkin A. Mechanosensitive channels: what can we learn from ‘simple’ model systems? Trends in Neurosciences. 2004 Jun 1;27(6):345–51.

5. Haswell ES, Phillips R, Rees DC. Mechanosensitive channels: what can they do and how do they do it? Structure (London, England : 1993). 2011 Oct 12;19(10):1356–69.

6. Cox CD, Bavi N, Martinac B. Bacterial Mechanosensors. Annual Review of Physiology. 2018;80(1):71–93.

7. Coste B, Mathur J, Schmidt M, Earley TJ, Ranade S, Petrus MJ, et al. Piezo1 and Piezo2 Are Essential Components of Distinct Mechanically Activated Cation Channels. Science. 2010 Oct 1;330(6000):55 LP – 60.

8. Hervieu GJ, Cluderay JE, Gray CW, Green PJ, Ranson JL, Randall AD, et al. Distribution and expression of TREK-1, a two-pore-domain potassium channel, in the adult rat CNS. Neuroscience. 2001;103(4):899–919.

9. Honoré E. The neuronal background K2P channels: focus on TREK1. Nature reviews Neuroscience. 2007 Apr;8(4):251–61.

10. Maingret F, Fosset M, Lesage F, Lazdunski M, Honoré E. TRAAK is a mammalian neuronal mechano-gated K+ channel. The Journal of biological chemistry. 1999 Jan;274(3):1381–7.

11. Dedman A, Sharif-Naeini R, Folgering JHA, Duprat F, Patel A, Honoré E. The mechano-gated K2P channel TREK-1. European Biophysics Journal. 2009;38(3):293–303.

12. Li W, Feng Z, Sternberg PW, Shawn Xu XZ. A C. elegans stretch receptor neuron revealed by a mechanosensitive TRP channel homologue. Nature. 2006;440(7084):684–7.

13. Wu LJ, Sweet TB, Clapham DE. International Union of Basic and Clinical Pharmacology. LXXVI. Current Progress in the Mammalian TRP Ion Channel Family. Pharmacological Reviews. 2010 Sep 1;62(3):381 LP – 404.

14. Nilius B, Szallasi A. Transient Receptor Potential Channels as Drug Targets: From the Science of Basic Research to the Art of Medicine. Sibley DR, editor. Pharmacological Reviews. 2014 Jul 1;66(3):676 LP – 814.

15. Jin P, Jan LY, Jan YN. Mechanosensitive Ion Channels: Structural Features Relevant to Mechanotransduction Mechanisms. Annual Review of Neuroscience. 2020 Feb 21;

16. Syeda R, Florendo MN, Cox CD, Kefauver JM, Santos JS, Martinac B, et al. Piezo1 Channels Are Inherently Mechanosensitive. Cell Reports. 2016;17(7):1739–46.

17. Bavi N, Richardson J, Heu C, Martinac B, Poole K. PIEZO1-Mediated Currents Are Modulated by Substrate Mechanics. ACS Nano. 2019 Nov 26;13(11):13545–59.

18. Xu J, Mathur J, Vessières E, Hammack S, Nonomura K, Favre J, et al. GPR68 Senses Flow and Is Essential for Vascular Physiology. Cell. 2018 Apr 19;173(3):762-775.e16.

19. Wiley SZ, Sriram K, Salmerón C, Insel PA. GPR68: An emerging drug target in cancer. Vol. 20, International Journal of Molecular Sciences. MDPI AG; 2019. p. 559.

20. Herzig M, Dasgupta P, Kaemmerer D, Sänger J, Evert K, Schulz S, et al. Comprehensive Assessment of GPR68 Expression in Normal and Neoplastic Human Tissues Using a Novel Rabbit Monoclonal Antibody. International journal of molecular sciences. 2019 Oct;20(21file:///C:/Users/psegeritz/Downloads/12955148.nbib).

21. Ludwig MG, Vanek M, Guerini D, Gasser JA, Jones CE, Junker U, et al. Proton-sensing G-protein-coupled receptors. Nature. 2003 Sep;425(6953):93–8.

22. Wei WC, Bianchi F, Wang YK, Tang MJ, Ye H, Glitsch MD. Coincidence Detection of Membrane Stretch and Extracellular pH by the Proton-Sensing Receptor OGR1 (GPR68). Current biology : CB. 2018 Dec;28(23):3815-3823.e4.

23. Sianati S, Kurumlian A, Bailey E, Poole K. Analysis of Mechanically Activated Ion Channels at the Cell-Substrate Interface: Combining Pillar Arrays and Whole-Cell Patch-Clamp . Vol. 7, Frontiers in Bioengineering and Biotechnology . 2019.

24. Kubanek J, Shi J, Marsh J, Chen D, Deng C, Cui J. Ultrasound modulates ion channel currents. Scientific Reports. 2016;6(1):24170.

25. Liao D, Li F, Lu D, Zhong P. Activation of Piezo1 mechanosensitive ion channel in HEK293T cells by 30 MHz vertically deployed surface acoustic waves. Biochemical and Biophysical Research Communications. 2019;518(3):541–7.

26. Prieto ML, Firouzi K, Khuri-Yakub BT, Maduke M. Activation of Piezo1 but Not Na(V)1.2 Channels by Ultrasound at 43 MHz. Ultrasound in medicine & biology. 2018 Jun;44(6):1217–32.

27. Ibsen S, Tong A, Schutt C, Esener S, Chalasani SH. Sonogenetics is a non-invasive approach to activating neurons in Caenorhabditis elegans. Nature Communications. 2015;6(1):8264.

28. Huang YS, Fan CH, Hsu N, Chiu NH, Wu CY, Chang CY, et al. Sonogenetic Modulation of Cellular Activities Using an Engineered Auditory-Sensing Protein. Nano Letters. 2020 Feb 12;20(2):1089–100.

29. Kriesi C, Steinert M, Marmaras A, Danzer C, Meskenaite V, Kurtcuoglu V. Integrated Flow Chamber System for Live Cell Microscopy . Vol. 7, Frontiers in Bioengineering and Biotechnology . 2019.

30. Xu L, Song X, Carroll G, You L. Novel in vitro microfluidic platform for osteocyte mechanotransduction studies. Integrative Biology. 2020 Dec 1;12(12):303–10.

31. Concilia G, Lai A, Thurgood P, Pirogova E, Baratchi S, Khoshmanesh K. Investigating the mechanotransduction of transient shear stress mediated by Piezo1 ion channel using a 3D printed dynamic gravity pump. Lab on a Chip. 2022 Jan 21;22(2):262–71.

32. Yen RT. Radial flow between two parallel discs. Kansas State University; 1965.

33. Wei WC, Bianchi F, Wang YK, Tang MJ, Ye H, Glitsch MD. Coincidence Detection of Membrane Stretch and Extracellular pH by the Proton-Sensing Receptor OGR1 (GPR68). Current Biology. 2018 Dec 3;28(23):3815-3823.e4.

34. Saxena H, Deshpande DA, Tiegs BC, Yan H, Battafarano RJ, Burrows WM, et al. The GPCR OGR1 (GPR68) mediates diverse signalling and contraction of airway smooth muscle in response to small reductions in extracellular pH. British journal of pharmacology. 2012 Jun;166(3):981–90.

35. Sforna L, Michelucci A, Morena F, Argentati C, Franciolini F, Vassalli M, et al. Piezo1 controls cell volume and migration by modulating swelling-activated chloride current through Ca2+ influx. Journal of Cellular Physiology. 2022 Mar 1;237(3):1857–70.

36. Dubin AE, Murthy S, Lewis AH, Brosse L, Cahalan SM, Grandl J, et al. Endogenous Piezo1 Can Confound Mechanically Activated Channel Identification and Characterization. Neuron. 2017 Apr 19;94(2):266-270.e3.

37. Ozkan AD, Gettas T, Sogata A, Phaychanpheng W, Zhou M, Lacroix JJ. Mechanical and chemical activation of GPR68 probed with a genetically encoded fluorescent reporter. Journal of Cell Science. 2021 Aug 17;134(16):jcs255455.

38. Kreß S, Schaller-Ammann R, Feiel J, Priedl J, Kasper C, Egger D. 3D Printing of Cell Culture Devices: Assessment and Prevention of the Cytotoxicity of Photopolymers for Stereolithography. Vol. 13, Materials. 2020.